Mesoporous Materials

Deutsche Ausgabe: DOI: 10.1002/ange.201605027
Internationale Ausgabe: DOI: 10.1002/anie.201605027

A Mesoporous Superlattice Consisting of Alternately Stacking Interstitial Nanospace within Binary Silica Colloidal Crystals

Yoshiyuki Kuroda, Yosuke Shimbo, Yasuhiro Sakamoto, Hiroaki Wada, and Kazuyuki Kuroda**

Abstract: *A novel class of nonclassical structures of mesoporous silica, namely a binary nanoparticle mesoporous superlattice (BNMS), is obtained by the assembly of silica nanospheres of different sizes into a binary colloidal crystal. The colloidal crystal has a CrB-type structure and consists of alternate stacks of unary fcc and binary AlB_2-type structures along the b axis and has four types of interstitial mesopores. The BNMS can be deposited on a substrate by dip coating to form an oriented thin film in which the direction of the superstructure (b axis) is perpendicular to the substrate.*

The design of superlattices is quite a useful way to access novel properties and integrated multifunctions. Superlattices with various compositions (e.g. metals, metal oxides, and semiconductors) and morphologies (e.g. bulk crystals, thin films, and nanoparticles) have so far been investigated;[1] however, most of them are not intended for the creation of nanospaces. Nanospace is used as a reservoir for molecules and nanoparticles, molecular transport channels, reaction fields, separation, etc.[2] Superlattices of nanospace are expected to be useful for achieving novel properties and/or multifunctional materials.

Mesoporous silica synthesized by the replication of surfactant micelles has periodically arranged uniform nanospace[3] and various ordered structures, such as lamellar, 2D hexagonal, gyroid, and 3D cage-type structures, have been reported.[3a] Recently, nonclassical nanospace structures, such as chiral,[4] intergrowth,[5] and quasicrystalline[6] structures, have also been generated, whereas an ordered superlattice of nanospace (namely mesoporous superlattice) has not been reported.

Mesoporous superlattices are expected to be fabricated by alternately stacking mesoporous silica with different structures. Wiesner and co-workers have reported the heteroepitaxial growth of surfactant-templated mesoporous silica;[7] however, it is not applicable for controlling the formation of mesoporous superlattices because the thickness of each mesoporous domain is much larger than unit-cell parameters and cannot be controlled. In addition, the method is applicable only for nanoparticles. The macroscopic alignment of mesoporous superlattices (e.g. films) is essential for the use of such unique superstructures.

Colloidal crystals consisting of monodispersed silica nanospheres with interstitial nanospace are regarded as mesoporous silica.[8,9] Oriented thin films of mesoscale colloidal crystals have been reported.[10] In unary systems, monodispersed silica nanospheres are usually assembled into face-centered cubic (fcc) and/or hexagonal close-packed (hcp) structures. We[11,12] as well as Snyder and co-workers[9] have successfully prepared binary colloidal crystals (i.e. AlB_2-,[9,11] $NaZn_{13}$-,[9,11–13] and NaCl-type[9] structures; see Figure S1 in the Supporting Information) by combining different-sized nanospheres with strictly controlled particle number ratios. The coexistance of nanostructures with different geometries is difficult to observe in the surfactant system because surfactant micelles readily reorganize into a single phase.[14] Such a coexistance of different nanostructures is possible in a colloidal crystal system when rigid nanospheres are used. Accordingly, the assembly of silica nanospheres is an ideal strategy for the formation of a superlattice of nanospace. Diverse binary nanoparticle superlattices (BNSLs) have been reported based on nanoparticles modified with alkyl ligands;[1d] however, their assembled structure often collapses upon heating. The use of silica nanospheres is essential for the construction of mesoporous materials.

Herein we report a binary nanoparticle mesoporous superlattice (BNMS) formed by assembling silica nanospheres of different sizes. A novel binary colloidal crystal **AB** (denoted as CC_{AB}) with a CrB-type structure (*Cmcm*, SG63; Figure 1 a; see Table S1 for structural parameters) was formed as a flake and an oriented thin film. The symbols **A** and **B** denote larger (32.9 nm) and smaller (16.9 nm) nanospheres, respectively. The CrB-type structure consists of alternately stacked layers of unary and binary colloidal crystals (Figures 1 b,c) with a large periodicity (lattice constant *b* of 95.0 nm). Each colloidal crystalline layer possesses

[*] Dr. Y. Kuroda
Waseda Institute for Advanced Study, Waseda University
1-6-1 Nishiwaseda, Shinjuku-ku
Tokyo 169-8050 (Japan)
E-mail: y-kuroda@aoni.waseda.jp
Y. Shimbo, Prof. H. Wada, Prof. K. Kuroda
Department of Applied Chemistry, Waseda University
3-4-1 Okubo, Shinjuku-ku, Tokyo 169-8555 (Japan)
E-mail: kuroda@waseda.jp
Prof. Y. Sakamoto
PRESTO, Japan, Science and Technology Agency (JST)
4-1-8 Honcho, Kawaguchi, Saitama 332-0012 (Japan)
and
Department of Physics, Osaka University
1-1 Machikaneyamacho, Toyonaka-shi, Osaka 560-0043 (Japan)
Prof. K. Kuroda
Kagami Memorial Research Institute for Science and Technology
Waseda University, 2-8-26 Nishiwaseda
Shinjuku-ku, Tokyo 169-0051 (Japan)

Supporting information for this article can be found under: http://dx.doi.org/10.1002/anie.201605027.

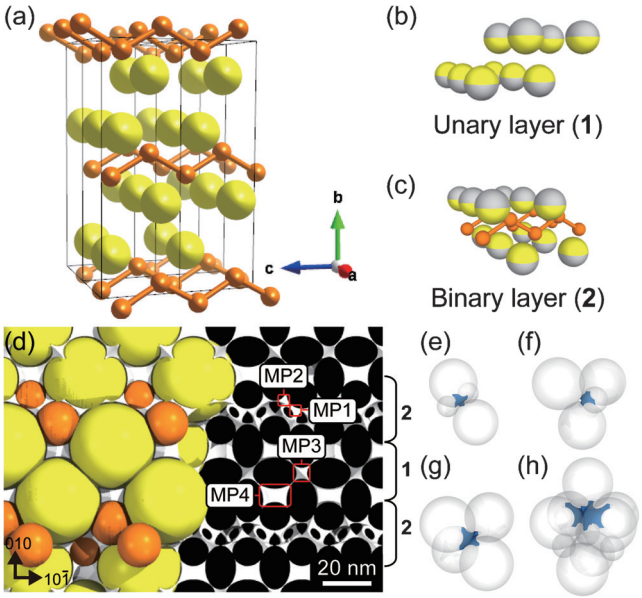

Figure 1. Structural models of a) the CrB-type structure, b) the unary layer, and c) the binary layer. Yellow and orange spheres indicate **A** and **B**, respectively. The sizes of the spheres are reduced for clarity. d) Model of interstitial nanospace in the CrB-type structure projected along the [101] zone axis, showing e) MP1, f) MP2, g) MP3, and h) MP4. The interstitial mesopores are indicated by white regions in (d) or blue regions in (e)–(h). The unary and binary layers are indicated by 1 and 2, respectively.

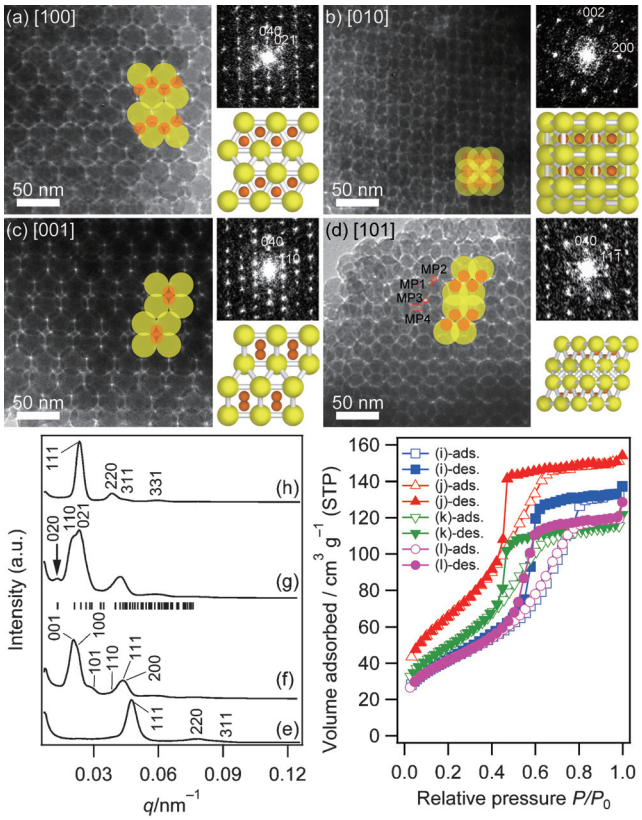

Figure 2. TEM images of CC_{AB} taken along the a) [100], b) [010], c) [001], and d) [101] axes. The insets show (upper right) the corresponding FFT images and (lower right) the structural models. **A** and **B** are depicted as yellow and orange circles/spheres, respectively. The sizes of the spheres are reduced for clarity. SAXS profiles of the colloidal crystals e) CC_B, f) CC_{AB2}, g) CC_{AB}, and h) CC_A. The mesopores are marked with red rectangles in (d). The bars below (g) indicate the calculated diffraction angles of the CrB-type structure. N_2 adsorption/desorption isotherms of i) CC_A, j) CC_B, k) CC_{AB2}, and l) CC_{AB}.

specific interstitial mesopores and, hence, CC_{AB} is a BNMS with a new class of nonclassical structure.

It is known that the phase stability of a hard-sphere colloidal crystal depends on the packing density of the silica nanospheres, that is, a denser structure is more stable.[16] The stabilities of various structures have been calculated by varying the size ratio (D_B/D_A, where D_A and D_B denote the diameters of **A** and **B**, respectively) and the particle number ratio (n_B/n_A, where n_A and n_B denote the numbers of **A** and **B**, respectively). The highest stability of the CrB-type structure was predicted when D_B/D_A is around 0.527 and n_B/n_A is 1.0.[16] The packing density at $D_B/D_A = 0.527$ is 0.7634, which is larger than that of a unary colloidal crystal with a fcc/hcp structure (0.74).[15a] We used silica nanospheres with $D_A = 32.9$ nm (standard deviation (σ) = 2.4 nm) and $D_B = 16.9$ nm (σ = 1.7 nm), where D_B/D_A is 0.514. These sizes are experimentally easy to control and appropriate for the formation of mesoscale interstitial nanospaces.[16] Since the size and number ratios of the silica nanospheres are adjusted to those specific to the formation of the CrB-type structure, the formation of the NaCl- and AlB_2-type structures are effectively suppressed.

A flake of CC_{AB} was prepared by evaporating a dispersion containing a 1:1 mixture of the silica nanospheres **A** and **B** (see the Experimental Section for details). The procedure is facile and allows production on a large (gram) scale. The transmission electron microscopy (TEM) images of CC_{AB} clearly show periodically arranged silica nanospheres (Figure 2a–d). The arrangements are consistent with the structural models, and the fast Fourier transform (FFT) images satisfy the reflection conditions of the *Cmcm* space group.[17] The lattice constants estimated by the FFT images are $a = c =$ 31.3 nm and $b = 95.0$ nm. These values are slightly smaller than those expected from the original particle sizes ($a = c =$ 32.9 nm and $b = 103.5$ nm), which is probably due to shrinkage arising from condensation of the silica. If **A** is closely packed, the lattice constant b is described by the equation $b = (\sqrt{2}+\sqrt{3})a$. The obtained lattice constants suggest a small contraction along the b axis. The unit cell is slightly distorted from the ideal orthorhombic cell, which is probably caused by the strain during solvent evaporation and/or thermal treatment. Such a distortion was also observed in our previous study for the AlB_2- and $NaZn_{13}$-type structures.[11]

The small-angle X-ray scattering (SAXS) profile of CC_{AB} was compared with those of other colloidal crystals (Figure 2e–h). A unary colloidal crystal consisting of only **A** and the one consisting of only **B** are denoted as CC_A and CC_B, respectively. A binary colloidal crystal $\mathbf{AB_2}$ is denoted as CC_{AB2}. A small diffraction peak at $q = 0.013$ nm^{-1} ($d = 48$ nm) attributable to the 020 reflection of the CrB-type structure was observed only in the profile of CC_{AB} (Figure 2g). The

peak at the lowest angle clearly shows that only CC_{AB} possesses the large periodicity. The main peaks are also consistent with the 110 and 021 reflections. Full assignment was not successful for the flake because of overlapping of the peaks, whereas the grazing-incidence (GI) SAXS pattern of an oriented thin film (described later) can be successfully assigned to the CrB-type structure.

The CrB-type structure consists of alternately stacked layers with a large periodicity (Figure 1 a). The half-cell of the fcc structure (unary layer; Figure 1 b) and a unit cell of the AlB_2-type structure (binary layer; Figure 1 c) are stacked layer-by-layer, sharing the (100) facet of the fcc structure and the (100) facet of the AlB_2-type structure. A zig-zag one-dimensional arrangement of **B** exists within the binary layer. The CrB-type structure possesses four characteristic interstitial mesopores (MPs) of different sizes (Figures 1 d). MP1 and MP2 are surrounded with **A** and **B** in the binary layer (Figures 1 e,f). MP3 and MP4 correspond to the tetrahedral and octahedral interstices, respectively, mainly surrounded by **A** in the unary layer (Figures 1 g,h). These mesopores are alternately stacked along the *b* axis.

The interstitial mesopores and the layer-by-layer structure were directly observed by high-resolution scanning electron microscopy (HRSEM; Figure 3). The observed facets, consisting only of **A**, are the laterally (along the *a*,*b* plane) cleaved facets of the unary layer (indicated as 1 in Figure 3). The facets consisting of **A** and **B** are the cleaved facets of the binary layer (indicated as 2 in Figure 3). The unary and binary layers are alternately stacked. A lateral shift vector in the *a*,*c* plane (*a*, *c*) from the binary layer to the unary layer is (0, 0.5), and that from the unary layer to the binary layer is (0.5, 0.5). They are consistent with the CrB-type structure. Thus, we conclude that CC_{AB} possesses a CrB-type structure with alternately stacked interstitial nanospace.

The porosities of the unary and binary colloidal crystals (CC_A, CC_B, CC_{AB2}, and CC_{AB}) were investigated by N_2 adsorption experiments (Figures 2 i–l). All samples show type IV isotherms, which is consistent with the existence of the interstitial mesopores. The total pore volume of CC_{AB} is smaller than those of CC_A and CC_B, thus indicating a higher packing density in CC_{AB} than in CC_A and CC_B (Table S2). In addition, the packing density of CC_{AB} is slightly smaller than that of CC_{AB2}, which is consistent with the proposed structural models. The calculated packing densities are smaller than the theoretical values, which is probably due to loose packing arising from the distribution of different sized particles and/or surface roughness.

The definition of the sizes of interstitial mesopores surrounded by convex surfaces is difficult and there are no models which describe the exact size distribution of such interstitial pores, whereas the BJH pore size should reflect the relative size of the nanospace.[9] The peak tops of the BJH pore size distribution curves of CC_A, CC_B, CC_{AB2}, and CC_{AB} are approximately 7 nm, 4 nm, 4 nm, and 6 nm, respectively (Figure S2). The peak at about 6 nm in the pore size distribution curve of CC_{AB} should contain the contribution from MP1–MP4. The pore sizes of MP3 and MP4 are almost the same as those of CC_A, whereas MP1 and MP2 are much smaller. Therefore, the slightly smaller pore size compared to

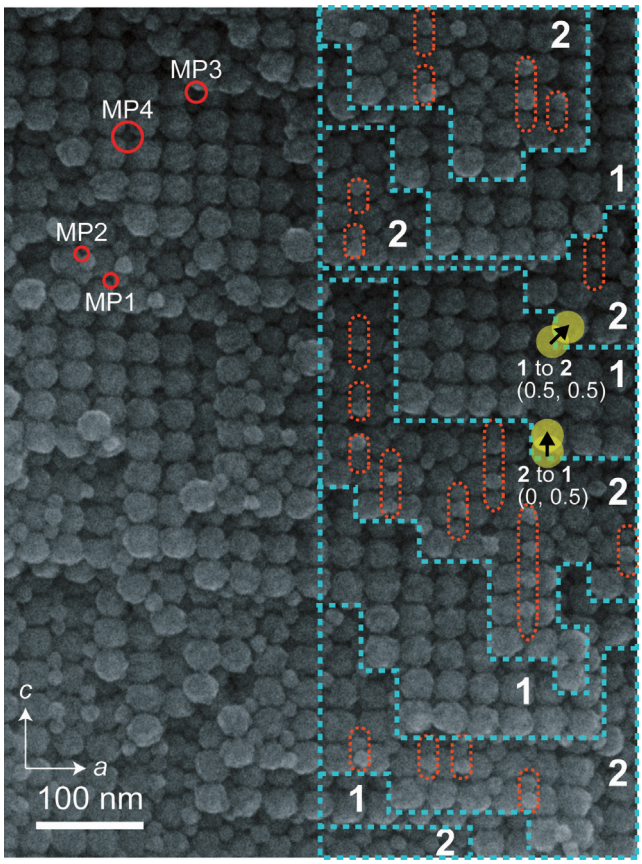

Figure 3. HRSEM image of CC_{AB} viewed along the [010] zone axis. Unary and binary layers are indicated by 1 and 2, respectively, and marked by blue dashed lines in the right side of the image. Red circles indicate the interstitial mesopores. Red dashed areas indicate one-dimensionally arranged **B**. Shift vectors are indicated by yellow circles with arrows.

that of CC_A is reasonable. The lowest pressure of the hysteresis loop usually corresponds to the size of the narrowest part of interstitial mesopores or cavitation.[18] The hysteresis of CC_{AB} is closed at a lower pressure than that of CC_A, and the lowest pressure is almost the same as those of CC_B and CC_{AB2}, which is consistent with the presence of small mesopores (MP1 and MP2) in CC_{AB}.

The one-dimensional zig-zag chains of **B** are almost uniaxially oriented (Figure S3 a). The zig-zag chains are aligned in at least 17 unit cells (Figure S3 b), although the layer rotated 90° around the *b* axis (rotated binary layer) is possibly inserted instead of the binary layer because both unary and binary layers possess the same tetragonal arrangement of **A**.

The CrB-type structure can be classified as the insertion of periodically ordered stacking faults (unary layer) in the AlB_2-type structure. Figure S4 shows the TEM image of the AlB_2-type binary colloidal crystal.[10] Stacking faults corresponding to the insertion of the unary layer in the AlB_2-type structure were observed. Thus, the formation of the CrB-type structure corresponds to periodic insertion of unary layers in the AlB_2-type structure. In addition, rotated binary layers were also observed.

The self-assembling method presented here is applicable to the fabrication of an oriented thin film that is deposited on a silicon substrate by dip coating. Cracks arising from shrinkage during the drying process were observed (Figure S5). The cross-sectional and surface HRSEM images of the thin film show the CrB-type structure (Figure 4a,b). The

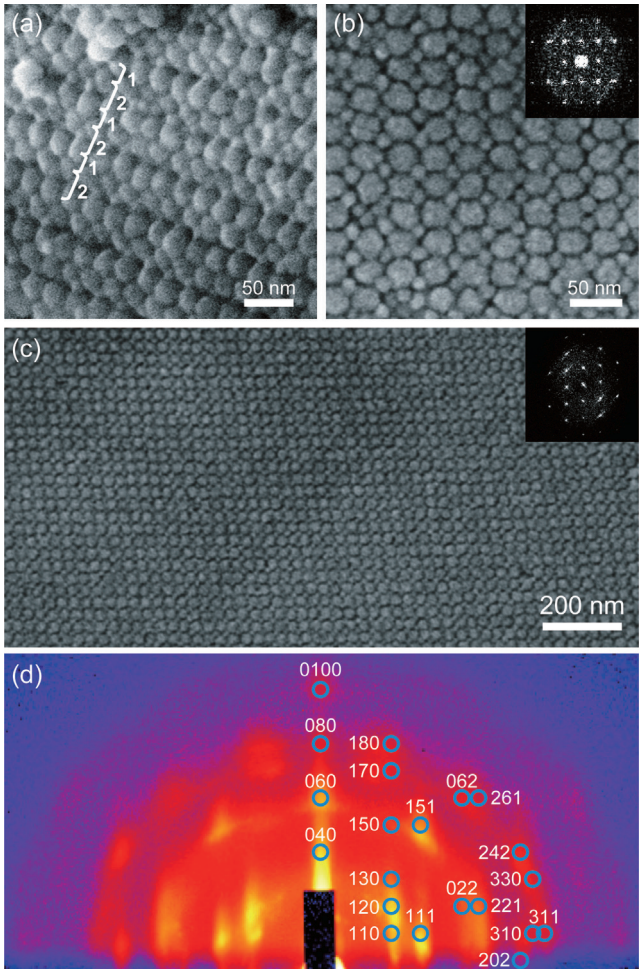

Figure 4. a) Cross-sectional and b,c) surface HRSEM images of a CC_{AB} thin film. The insets in (b,c) show the corresponding FFT patterns. d) GI-SAXS pattern of the CC_{AB} thin film.

thickness was about 2.5 μm (Figure S6). The surface of the thin film is flat and shows a facet of the binary layer over a very wide area (Figure 4c), thus suggesting that the *b* axis is perpendicular to the substrate. The GI-SAXS pattern of the thin film shows many spots which are assignable to the CrB-type structure, whose *b* axis is perpendicular to the substrate (Figure 4d). This is useful for the layer-by-layer assembly of functional materials on a substrate as was demonstrated by the successful fabrication of an oriented thin film of BNMS. The long-range periodicity of the CrB-type structure is mostly along the normal direction to the substrate.

BNMS has several structural and textural characteristics different from conventional mesoporous silica. BNMS has three-dimensionally ordered interstitial mesopores surrounded by convex surfaces. Such interstitial mesopores possess wide entrances and are highly accessible. Pore walls consisting of silica nanospheres are much thicker than those of conventional mesoporous silica. The pore walls are useful as templates of mesoporous materials with different compositions and can be crystallized into single-crystalline quartz with unique properties (chemical stability, hardness, and piezoelectricity).[8] On the other hand, various morphologies have been achieved for conventional mesoporous silica synthesized by sol-gel methods. The morphological control of colloidal crystals by using BNMS is an important issue to be tackled in the future.

BNMS is expected to be useful as a template for nanoparticle superlattices. It is well-known that plasmonic properties of metal nanoparticles are highly dependent on their particle sizes.[19] By depositing metal nanoparticles in the interstitial mesopores of BNMSs, the arrangement, size, and distance of metal nanoparticles can be controlled. If surface-functionalized and nonfunctionalized nanospheres (e.g. nonfunctionalized **A** and functionalized **B**) are assembled into a BNMS, the functional groups will be mainly on the surfaces of MP1 and MP2. The selective deposition of different metal/semiconductor nanoparticles in different mesopores is expected.

In conclusion, a binary nanoparticle, mesoporous superlattice—a novel nonclassical mesoporous silica—was demonstrated by assembling binary silica nanospheres into a CrB-type structure. The structure consists of alternately stacking unary fcc and binary AlB_2-type colloidal crystalline layers, thereby forming four types of interstitial mesopores arranged periodically along the *b* axis. The self-assembling process is applicable to the formation of an oriented thin film of a CrB-type colloidal crystal, in which the *b* axis is perpendicular to the substrate. The present material does not require any complex processes and can be prepared in bulk. We believe that the discovery of BNMS will open a new door for the control of complex mesoporous structures, integration of functions, and novel templated syntheses.

Experimental Section

Materials: L-Lysine was purchased from Sigma–Aldrich Co. LLC. Tetraethoxysilane (TEOS), ethanol, and sulfuric acid were purchased from Wako Pure Chemical Ind. Ltd. All reagents were used as received.

Preparation of colloidal crystals: Monodispersed silica nanospheres with different sizes were prepared by the seed-growth method as reported previously.[11] The sizes of the nanospheres **A** and **B** were 32.9 nm ($\sigma = 2.4$ nm) and 16.9 nm ($\sigma = 1.7$ nm), respectively (estimated by SAXS). Unary colloidal crystals CC_A and CC_B were obtained by evaporating the dispersions of the nanospheres under ambient conditions (22–25 °C, 30–70 % relative humidity), followed by calcination at 550 °C for 6 h. The binary colloidal crystals CC_{AB} were obtained by mixing the dispersions of nanospheres **A** and **B** to adjust the number ratio to 1:1 before the evaporation and calcination.

Preparation of binary colloidal crystal thin film: A clean silicon wafer was first immersed in conc. sulfuric acid for more than 1 day to obtain a hydrophilic surface, followed by washing with deionized water. The dispersions of nanospheres **A** and **B** were mixed to adjust the numerical ratio to 1:1. A silicon wafer was dip-coated into the mixture using an EINTESLA ND-0407 dip coater at a lifting speed of

0.2 μm s^{-1}. The as-obtained thin film was calcined at 600 °C for 6 h under air.

Characterization: SAXS measurements were performed on a Rigaku Nanoviewer apparatus at 40 kV and 30 mA, using a Pilatus 2D detector. The camera length was 1300 mm. For the transmission optical system, samples were roughly crushed in a mortar and mounted in a sample holder. When the samples were finely crushed, the enhanced scattering near the direct beam prohibited the observation of weak low-angle peaks. The GI-SAXS patterns were obtained at an incident angle of 0.1°. TEM images were recorded on a JEOL JEM-2010 microscope at an accelerating voltage of 200 kV. Samples were dispersed in ethanol and dried on a holey carbon-coated Cu grid. HRSEM images were recorded on a Hitachi S-5500 microscope at an accelerating voltage of 3 or 30 kV. The samples were observed without metal coating. N_2 adsorption/desorption isotherms were measured on a Quantachrome Instruments Autosorb-1 apparatus at −196 °C. Samples were heated at 120 °C for 3 h prior to measurement.

Acknowledgements

We thank Prof. Atsushi Shimojima (Waseda University) and Shintaro Hara (Waseda University) for fruitful discussions. We also appreciate Takeshi Mino (Waseda Univeristy) for his assistance with GI-SAXS measurements. This work was supported in part by Grants-in-Aid for Scientific Research (No. 26810118 and No. 26248060), Mizuho Foundation for the Promotion of Science, Research Fund from JX Nippon Oil & Energy for Young Scientists, and Futaba Electronics Memorial Foundation.

Keywords: colloidal crystals · mesoporous materials · nanoparticles · silica · thin films

How to cite: *Angew. Chem. Int. Ed.* **2016**, *55*, 10702–10706
Angew. Chem. **2016**, *128*, 10860–10864

[1] a) B. Y. Jin, J. B. Ketterson, *Adv. Phys.* **1989**, *38*, 189–366; b) N.-B. Ming, *Adv. Mater.* **1999**, *11*, 1079–1089; c) A. Wacker, *Phys. Rep.* **2002**, *357*, 1–111; d) E. V. Shevchenko, D. V. Talapin, N. A. Kotov, S. O'Brien, C. B. Murray, *Nature* **2006**, *439*, 55–59.

[2] M. E. Davis, *Nature* **2002**, *417*, 813–821.

[3] a) Y. Wan, D. Zhao, *Chem. Rev.* **2007**, *107*, 2821–2860; b) A. Taguchi, F. Schüth, *Microporous Mesoporous Mater.* **2005**, *77*, 1–45; c) Z. Wu, D. Zhao, *Chem. Commun.* **2011**, *47*, 3332–3338; d) E. Yamamoto, K. Kuroda, *Bull. Chem. Soc. Jpn.* **2016**, *89*, 501.

[4] a) S. Che, Z. Liu, T. Ohsuna, K. Sakamoto, O. Terasaki, T. Tatsumi, *Nature* **2004**, *429*, 281–284; b) H. Qiu, Y. Sakamoto, O. Terasaki, S. Che, *Adv. Mater.* **2008**, *20*, 425–429.

[5] a) Y. Sakamoto, L. Han, S. Che, O. Terasaki, *Chem. Mater.* **2009**, *21*, 223–229; b) L. Han, Y. Sakamoto, S. Che, O. Terasaki, *Chem. Eur. J.* **2009**, *15*, 2818–2825.

[6] C. Xiao, N. Fujita, K. Miyasaka, Y. Sakamoto, O. Terasaki, *Nature* **2012**, *487*, 349–353.

[7] T. Suteewong, H. Sai, R. Hovden, D. Muller, M. S. Bradbury, S. M. Gruner, U. Wiesner, *Science* **2013**, *340*, 337–341.

[8] a) T. Yokoi, Y. Sakamoto, O. Terasaki, Y. Kubota, T. Okubo, T. Tatsumi, *J. Am. Chem. Soc.* **2006**, *128*, 13664–13665; b) Y. Kuroda, Y. Yamauchi, K. Kuroda, *Chem. Commun.* **2010**, *46*, 1827–1829; c) Y. Kuroda, K. Kuroda, *Angew. Chem. Int. Ed.* **2010**, *49*, 6993–6997; *Angew. Chem.* **2010**, *122*, 7147–7151; d) T. Matsuno, Y. Kuroda, M. Kitahara, A. Shimojima, H. Wada, K. Kuroda, *Angew. Chem. Int. Ed.* **2016**, *55*, 6008–6012; *Angew. Chem.* **2016**, *128*, 6112–6116.

[9] S.-C. Kung, C.-C. Chang, W. Fan, M. A. Snyder, *Langmuir* **2014**, *30*, 11802–11811.

[10] M. A. Snyder, J. A. Lee, T. M. Davis, L. E. Scriven, M. Tsapatsis, *Langmuir* **2007**, *23*, 9924–9928.

[11] Y. Kuroda, Y. Sakamoto, K. Kuroda, *J. Am. Chem. Soc.* **2012**, *134*, 8684–8692.

[12] Y. Sakamoto, Y. Kuroda, S. Toko, T. Ikeda, T. Matsui, K. Kuroda, *J. Phys. Chem. C* **2014**, *118*, 15004–15010.

[13] The $NaZn_{13}$-type structure also consists of a superlattice with a cubic structure, although most of the mesopores have a similar size. The CrB-type structure has four types of nanospaces with similar abundance.

[14] Bimodal assembly of different surfactants have been achieved in only limited systems, see O. Sel, D. Kuang, M. Thommes, B. Smarsly, *Langmuir* **2006**, *22*, 2311–2322; F. Gao, C. Lian, L. Zhou, H. Liu, J. Hu, *Langmuir* **2014**, *30*, 11284–11291.

[15] a) J. K. Kummerfeld, T. S. Hudson, P. Harrowell, *J. Phys. Chem. B* **2008**, *112*, 10773–10776; b) L. Filion, M. Marechal, B. van Oorschot, D. Pelt, F. Smallenburg, M. Dijkstra, *Phys. Rev. Lett.* **2009**, *103*, 188302.

[16] The particle size was important in practice. When larger nanospheres ($D_A = 60$ nm and $D_B = 30$ nm) were used, unary colloidal crystals of **A** and disordered aggregates of both **A** and **B** were mainly formed instead of the CrB-type structure. It is proposed that **A** assembled earlier than **B** during the evaporation because of the difference in their zeta potentials (see Ref. [9]). The use of small nanospheres with similar zeta potentials is necessary to assemble **A** and **B** at the same time.

[17] Reflection conditions for *Cmcm* are as follows: hkl: $h+k=2n$; $0kl$: $k=2n$; $h0l$: $h,l=2n$; $hk0$: $h+k=2n$; $h00$: $h=2n$; $0k0$: $k=2n$; $00l$: $l=2n$.

[18] P. I. Ravikovitch, A. V. Neimark, *Langmuir* **2002**, *18*, 9830–9837.

[19] M. R. Jones, K. D. Osberg, R. J. Macfarlane, M. R. Langille, C. A. Mirkin, *Chem. Rev.* **2011**, *111*, 3736–3827.

Received: May 23, 2016
Published online: July 28, 2016

